Black hole formation and growth: simulations in general relativity

By STUART L. SHAPIRO[1,2]

[1]Department of Physics, University of Illinois at Urbana-Champaign, Urbana, IL 61801, USA

[2]Department of Astronomy and National Center for Supercomputing Applications, University of Illinois at Urbana-Champaign, Urbana, IL 61801, USA

Black holes are popping up all over the place: in compact binary X-ray sources and GRBs, in quasars, AGNs and the cores of all bulge galaxies, in binary black holes and binary black hole-neutron stars, and maybe even in the LHC! Black holes are strong-field objects governed by Einstein's equations of general relativity. Hence general relativistic, numerical simulations of dynamical phenomena involving black holes may help reveal ways in which black holes can form, grow and be detected in the universe. To convey the state-of-the art, we summarize several representative simulations here, including the collapse of a hypermassive neutron star to a black hole following the merger of a binary neutron star, the magnetorotational collapse of a massive star to a black hole, and the formation and growth of supermassive black hole seeds by relativistic MHD accretion in the early universe.

1. Introduction

Black holes are 'sighted' everywhere in the universe these days. Originally located in compact binary X-ray sources in the 1970's, the cosmic presence of black holes has expanded considerably in recent decades. They now are believed to be the central engines that power quasars, active galactic nuclei (AGNs) and gamma-ray bursts (GRBs). They are identified in the cores of all bulge galaxies. They are presumed to form signficant populations of compact binaries, including black hole-black hole binaries (BHBHs) and black hole-neutron star binaries (BHNSs). Black holes may even show up soon in the Large Hadron Collider!

Gravitationally, black holes are strong-field objects whose properties are governed by Einstein's theory of relativistic gravitation — general relativity. General relativistic simulations of gravitational collapse to black holes, BHBH mergers and recoil, black hole accretion, and other astrophysical phenomena involving black holes may help reveal how, when and where black holes form, grow and interact in the physical universe. As a consequence, such simulations can help identify the ways in which black holes can best be detected.

To illustrate how our understanding of black hole phenomena is sharpend by large-scale simulations in general relativity, we summarize in this paper the results of several recent computational investigations. The first few involve the formation of black holes from stellar collapse, while the last one concerns supermassive black hole growth via disk accretion. Most of these simulations utilize the tools of numerical relativity to solve Einstein's field equations of general relativity. So we shall begin with a brief overview of this important, rapidly maturing field.

2. Numerical Relativity and the $3+1$ Formalism

Most current work in numerical relativity is performed within the framework of the $3+1$ decomposition of Einstein's field equations using some adaptation of the standard ADM equations (Arnowitt, Deser & Misner 1962). In this framework spacetime is sliced

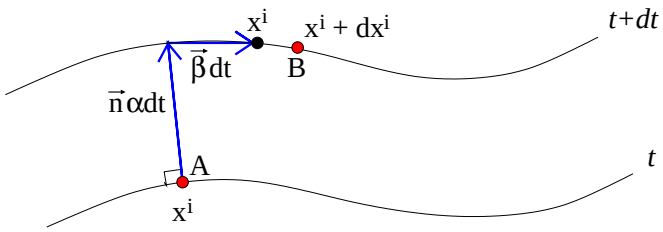

FIGURE 1. 3+1 decomposition of spacetime.

up into a sequence of spacelike hypersurfaces of constant time t, appropriate for solving an initial-value problem. Consider two such time slices separated by an infinitesimal interval dt as shown in Fig 1. The spacetime metric measures the invariant interval between neighboring points A and B on the two slices according to

$$ds^2 = -\alpha^2 dt^2 + \gamma_{ij}(dx^i + \beta^i dt)(dx^j + \beta^j dt) \ , \tag{2.1}$$

where γ_{ij} is the spatial 3-metric on a time slice, α is the lapse function determining the proper time between the slices as measured by a time-like normal observer n^a at rest in the slice, and β^i is the shift vector, a spatial 3-vector that describes the relabeling of the spatial coordinates of points in the slice. The gravitational field satisfies the Hamiltonian and momentum *constraint equations* on each time slice, including the initial slice at $t = 0$:

$$R + K^2 - K_{ij}K^{ij} = 16\pi\rho \quad \text{(Hamiltonian)} \ , \tag{2.2}$$

$$D_j(K^{ij} - \gamma^{ij}K) = 8\pi S^i \quad \text{(momentum)} \ . \tag{2.3}$$

Here $R = R^i{}_i$ is the scalar curvature on the slice, R_{ij} is the 3-Ricci tensor, K_{ij} is the extrinsic curvature, K is its trace, and D_j is the covariant derivative operator on the slice. The quantities ρ and S^i are the mass and momentum densities of the matter, respectively; such matter source terms are formed by taking suitable projections of the matter stress-energy tensor T^{ab} with respect to the normal observer. Included in this stress-energy tensor are contributions from all the nongravitational sources of mass-energy, which we are simply calling the "matter" (e.g., baryons, electromagnetic fields, neutrinos, etc.).

A gravitational field satisfying the constraint equations on the initial slice can be determined at future times by integrating the *evolution equations*,

$$\partial_t \gamma_{ij} = -2\alpha K_{ij} + D_i\beta_j + D_j\beta_i \ , \tag{2.4}$$

$$\begin{aligned} \partial_t K_{ij} = {} & \alpha(R_{ij} - 2K_{ik}K^k{}_j + KK_{ij}) - D_iD_j\alpha \\ & + \beta^k\partial_k K_{ij} + K_{ik}\partial_j\beta^k + K_{kj}\partial_i\beta^k - 8\pi\alpha(S_{ij} - \frac{1}{2}\gamma_{ij}(S - \rho)) \ , \end{aligned} \tag{2.5}$$

where S and S_{ij} are additional matter source terms. The evolution equations guarantee that the field equations will automatically satisfy the constraints on all future time slices identically, provided they satisfy them on the initial slice. Of course, this statement applies to the analytic set of equations and not necessarily to their numerical counterparts.

Note that the 3+1 formalism prescribes no equations for α and β^i. These four functions embody the four-fold gauge (coordinate) freedom inherent in general relativity. Choosing them judiciously, especially in the presence of black holes, is one of the main challenges of numerical relativity.

2.1. *The BSSN Scheme*

During the past decade, significant improvement in our ability to numerically integrate Einstein's equations stably in full $3+1$ dimensions has been achieved by recasting the original ADM system of equations. One such reformulation is the so-called BSSN scheme (Shibata & Nakamura 1995; Baumgarte & Shapiro 1999). In this scheme, the physical metric and extrinsic curvature variables are replaced in favor of the conformal metric and extrinsic curvature, in the spirit of the "York-Lichnerowicz" split (Lichnerowicz 1944; York 1971):

$$\tilde{\gamma}_{ij} = e^{-4\phi}\gamma_{ij}, \quad \text{where} \quad e^{4\phi} = \gamma^{1/3} \ , \tag{2.6}$$

$$\tilde{A}_{ij} = \tilde{K}_{ij} - \frac{1}{3}\tilde{\gamma}_{ij}K \ . \tag{2.7}$$

Here a tilde $\tilde{}$ denotes a conformal quantity and γ is the determinant of γ_{ij}. At the same time, a connection function $\tilde{\Gamma}^i$ is introduced according to

$$\tilde{\Gamma}^i \equiv \tilde{\gamma}^{jk}\tilde{\Gamma}^i{}_{jk} = -\partial_j\tilde{\gamma}^{ij} \ . \tag{2.8}$$

The quantities that are independently evolved in this scheme are now $\tilde{\gamma}_{ij}, \tilde{A}_{ij}, \phi, K$ and $\tilde{\Gamma}^i$. The advantage is that the Riemann operator appearing in the evolution equations (cf. eqn. (2.5)) takes on the form,

$$\tilde{R}_{ij} = -\frac{1}{2}\underbrace{\tilde{\gamma}^{lm}\partial_m\partial_l\tilde{\gamma}_{ij}}_{\text{`}Laplacian\text{`}} + \underbrace{\tilde{\gamma}_{k(i}\partial_{j)}\tilde{\Gamma}^k}_{\text{remaining 2nd derivs}} + \cdots \ . \tag{2.9}$$

Thus the principal part of this operator, $\tilde{\gamma}^{lm}\partial_m\partial_l\tilde{\gamma}_{ij}$ is that of a Laplacian acting on the components of the metric $\tilde{\gamma}_{ij}$. All the other second derivatives of the metric have been absorbed in the derivatives of the connection functions. The coupled evolution equations for $\tilde{\gamma}_{ij}$ and $\tilde{A}_{ij}$ (cf. eqns. (2.4) and (2.5) then reduce essentially to a wave equation,

$$\partial_t^2\tilde{\gamma}_{ij} \sim \partial_t\tilde{A}_{ij} \sim \tilde{R}_{ij} \sim \nabla^2\tilde{\gamma}_{ij} \ . \tag{2.10}$$

Wave equations not only reflect the hyperbolic nature of general relativity, but can be implemented numerically in a straight-forward and stable manner. By now, numerous simulations have demonstrated the dramatically improved stability achieved in the BSSN scheme over the standard ADM equations, and considerable effort has gone into explaining the improvement on theoretical grounds [see, e.g., Baumgarte & Shapiro 2003 for discussion and references]. Many of the recent BHBH merger calculations have been performed using this scheme, beginning with Campanelli *et al.* (2006) and Baker *et al.* (2006) (but see Pretorius 2005 for an alternative approach). The same is true for the simulations described below.

3. Binary Neutron Star Mergers and Hypermassive Stars

The protagonist of several different astrophysical scenarios probed by recent numerical simulations is a *hypermassive* star, typically a hypermassive neutron star (HMNS). A hypermassive star is an equilibrium fluid configuration that supports itself against gravitational collapse by *differential* rotation. Uniform rotation can increase the maximum mass of a nonrotating, spherical equilibrium star by at most $\sim 20\%$, but differential rotation can achieve a much higher increase (Baumgarte, Shapiro & Shibata 2000; Morrison, Baumgarte & Shapiro 2004). Dynamical simulations using the BSSN scheme demonstrate (Baumgarte, Shapiro & Shibata 2000) that hypermassive stars can be constructed that

are *dynamically* stable, provided the ratio of rotational kinetic to gravitational potential energy, β, is not too large; for $\beta \gtrsim 0.24$ the configuration is subject to a nonaxisymmetric dynamical bar instability (Shibata, Baumgarte & Shapiro 2000; Saijo *et al.* 2001). However, all hypermassive stars are *secularly* unstable to the redistribution of angular angular momentum by viscosity, magnetic braking, gravitational radiation, or any other agent that dissipates internal shear. Such a redistribution tends to drive a hypermassive star to uniform rotation, which cannot support the mass against collapse. Hence hypermassive stars are transient phenomena. Their formation following, for example, a NSNS merger, or core collapse in a massive, rotating star, may ultimately lead to a 'delayed' collapse to a black hole on secular (dissipative) timescales. Such a collapse will be accompanied inevitably by a delayed gravitional wave burst (Baumgarte, Shapiro & Shibata 2000; Shapiro 2000).

The above scenario has become very relevant in light of the most recent and detailed simulations in full general relativity of NSNS mergers. State-of-the-art, fully relativistic simulations of NSNSs have been performed by Shibata and his collaborators (Shibata, Taniguchi & Uryū 2003,2005; Shibata 2005; Shibata & Taniguchi 2006). They consider mergers of $n = 1$ polytropes, as well as configurations obeying a more realistic nuclear equation of state (EOS). They treat mass ratios Q_M in the range $0.9 \leqslant Q_M \leqslant 1$, consistent with the range of Q_M in observed binary pulsars with accurately determined masses (Thorsett & Chakrabarty 1999; Stairs 2004). The key result is that there exists a critical mass $M_{\rm crit} \sim 2.5 - 2.7 M_\odot$ of the binary system above which the merger leads to prompt collapse to a black hole, and below which the merger forms a hypermassive remnant. With the adopted EOS, the HMNS remnant undergoes delayed collapse in about ~ 100 ms and emits a delayed gravitational wave burst. Most interesting, prior to collapse, the remnant forms a triaxial bar when a realistic EOS is adopted (see Fig. 2) and the bar emits quasiperiodic gravitational waves at a frequency $f \sim 3 - 4$ kHz. Such a signal may be detectable by Advanced LIGO. It is interesting that for the adopted EOS, the mass $M_{\rm crit}$ is close to the value of the total mass found in each of the observed binary pulsars. Given that the masses of the individual stars in a binary can be determined by measuring the gravitational wave signal emitted during the adiabatic, inspiral epoch prior to plunge and merger, the detection (or absence) of any quasiperiodic emission from the hypermassive remnant prior to delayed collapse may significantly constrain models of the nuclear EOS.

The possibility that a HMNS remnant forms following a NSNS merger had been foreshadowed in earlier Newtonian simulations (Rasio & Shapiro 1994,1999; Zhuge, Centrella & McMillan 1996), in post-Newtonian simulations (Faber & Rasio 2000,2002) and in conformally flat general relativistic simulations (Faber, Grandclément & Rasio 2004). However, the recent fully relativistic simulations by Shibata, Taniguchi & Uryū (2003,2005), Shibata (2005) and Shibata & Taniguchi (2006) provide the strongest theoretical evidence of this phenomenon to date, although the details undoubtedly depend on the adopted EOS. Triaxial equilibria can arise only in stars that can support sufficiently high values of β exceeding the classical bifurcation point at $\beta \approx 0.14$; reaching such high values requires EOSs with adiabatic indicies exceeding $\Gamma \approx 2.25$ in Newtonian configurations, and comparable values in relativistic stars. It is not yet known whether the true nuclear EOS in neutron stars is this stiff, or what agent for redistributing angular momentum in a hypermassive star dominates (e.g., magnetic fields, turbulent viscosity or gravitational radiation). But it is already evident that hypermassive stars are likely to form from some mergers and that they will survive many dynamical timescales before undergoing delayed collapse. The recent measurement (Nice *et al.* 2005) of the mass of a neutron star in a neutron star-white dwarf binary of $M = 2.1 M_\odot$ establishes an observational lower

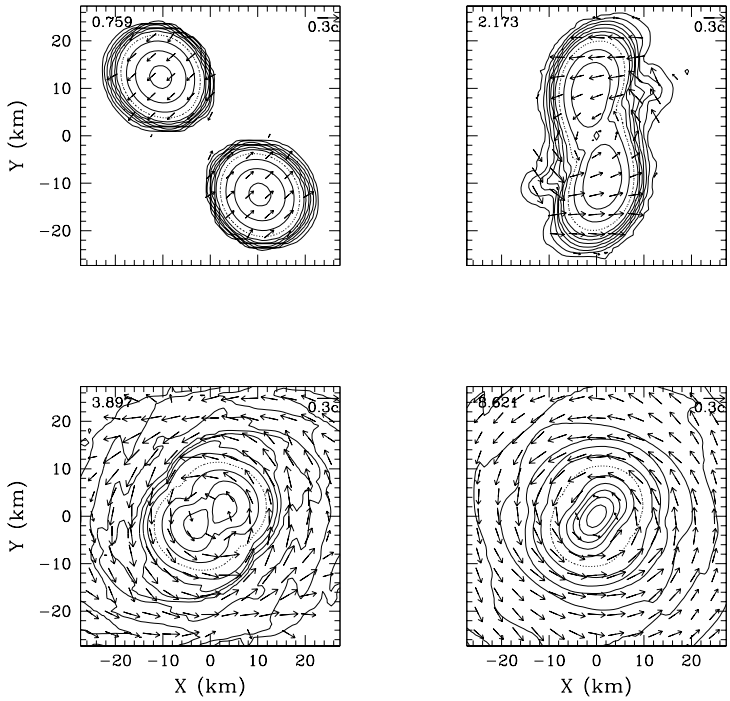

FIGURE 2. Formation of triaxial HMNS remnant following NSNS merger in $2.7M_\odot$ system. Snapshots of density contours are shown in the equatorial plane. The number in the upper left-hand corner denotes the elapsed time in ms; the initial orbital period is 2.11 ms. Vectors indicate the local velocity field. [From Shibata, Taniguchi and Uryū 2005.]

limit for the maximum mass of a neutron star; such a high value suggests that mergers in typical NSNSs may form hypermassive stars more often than undergoing prompt collapse.

3.0.1. *Collapse of a Magnetized HMNS*

The HMNSs found above may survive for many rotation periods. However, as we stated, on longer timescales magnetic fields will transport angular momentum and this will trigger gravitational collapse. Two important magnetohydrodynamic (MHD) mechanisms which transport angular momentum are magnetic braking (Baumgarte, Shapiro & Shibata 2000, Shapiro 2000, Cook, Shapiro & Stephens 2003, Liu & Shapiro 2003) and the magnetorotational instability (MRI; Velikhov 1959, Chandrasekhar 1960, Balbus & Hawley 1991,1998). Magnetic breaking transports angular momentum on the Alfvén time scale, $\tau_A \sim R/v_A \sim 1(B/10^{14}\ \mathrm{G})^{-1}$ s, where R is the radius of the HMNS. MRI occurs wherever angular velocity Ω decreases with cylindrical radius ϖ. This instability grows exponentially with an e-folding time of $\tau_{\rm MRI} \approx 4\,(\partial\Omega/\partial \ln \varpi)^{-1}$, independent of the field strength. For typical HMNSs considered here, $\tau_{\rm MRI} \sim 1$ ms. The length scale of the fastest growing unstable MRI modes, $\lambda_{\rm MRI}$, does depend on the field strength: $\lambda_{\rm MRI} \sim 3$ m $(\Omega/4000s^{-1})^{-1}$ $(B/10^{14}\mathrm{G}) \ll R$. When the MRI saturates, turbulence consisting of small-scale eddies often develops, leading to angular momentum transport on a timescale much longer than $\tau_{\rm MRI}$. The computational challenge of evolving an HMNS

is having sufficient spatial grid to resolve the MRI wavelength and sufficient integration time to follow the evolution on the long Alfvén timescale.

To determine the final fate of the HMNS, it is necessary to carry out MHD simulations in full general relativity. Such simulations have only recently become possible. Duez *et al.* (2005) and Shibata & Sekiguchi (2005) have developed new codes to evolve the coupled set of Einstein-Maxwell-MHD equations self-consistently. Our two codes have since been used to simulate the evolution of magnetized HMNSs (Duez *et al.* 2006a,2006b), and implications for short GRBs have been investigated (Shibata *et al.* 2006). Both codes give very similar results.

We assume axisymmetry and equatorial symmetry in all of these simulations. We use uniform computational grids with sizes up to 500×500 spatial zones in cylindrical coordinates. To model the remnant formed in binary merger simulations, we use as our initial data an equilibrium HMNS constructed from a $\Gamma = 2$ polytrope with mass M 1.7 times the spherical mass limit, or 1.5 times the limit for a uniformly rotating star built out of the same EOS. These are the typical values expected for a HMNS formed from a NSNS merger, for which $M \sim 2 \times 1.4 M_\odot = 2.8 M_\odot$. The differential rotation profile is chosen so that the ratio of equatorial to central Ω is $\sim 1/3$, comparable to what is found in simulations of NSNS mergers. (We find that an HMNS with a more realistic hybrid EOS rather than a polytrope evolves similarly; Duez *et al.* 2006b, Shibata *et al.* 2006) We add a seed poloidal magnetic field with strength proportional to the gas pressure. The initial magnetic pressure is set much smaller than the gas pressure, but not so small that $\lambda_{\rm MRI}$ cannot be resolved. Therefore, we set $\lambda_{\rm MRI} \approx R/10$, corresponding to $B \approx 10^{16}$ G and $\max(B^2/P) \sim 10^{-3}$. The resulting Alfvén timescale is about 16 central rotation periods, or $600M$.

In our evolutions, the effects of magnetic winding are reflected in the generation of a toroidal B field which grows linearly with time during the early phase of the evolution, and saturates on the Alfvén timescale. The effects of MRI are observed in an exponential growth of the poloidal field on the $\lambda_{\rm MRI}$ scale, a growth which saturates after a few rotation periods. The magnetic fields cause angular momentum to be transported outward, so that the core of the star contracts while the outer layers expand. After about 66 rotation periods, the core collapses to a black hole. Using the technique of black hole excision (see Duez, Shapiro & Yo 2004 and references therein) to remove the interior of the black hole, with its nasty spacetime singularity, and replace it with suitable boundary conditions on all the variables just inside the horizon, we continue the evolution to a quasi-stationary state. The final state consists of a black hole of irreducible mass $\sim 0.9M$ surrounded by a hot accreting torus with rest mass $\sim 0.1M$ and a magnetic field collimated along the rotation axis; see Fig. 3. At its final accretion rate, the torus should survive for $\sim$10ms. The torus is optically thick to neutrinos, and we estimate that it will emit $\sim 10^{50}$ergs in neutrinos before being accreted. We also find that the cone outside the black hole centered along the rotation axis is very baryon-poor. All these properties make this system a promising central engine for a short-hard GRB.

4. Black Holes as Central Engines for GRBs

The combined observations of *BATSE, Swift, HETE-2, Chandra* and the HST indicate that GRBs comprise at least two classes: long-soft and short-hard. Long-soft GRBs have characteristic timescales τ in the range $\tau \sim 2 - 10^3$s. They are found in star-forming regions (spirals) and some are observed to be associated with supernovae. The favored model for the progenitor of a long-soft GRB is the collapse of a massive, rotating, magnetized star to a black hole ('collapsar'; MacFadyen & Woosley 1999). By contrast,

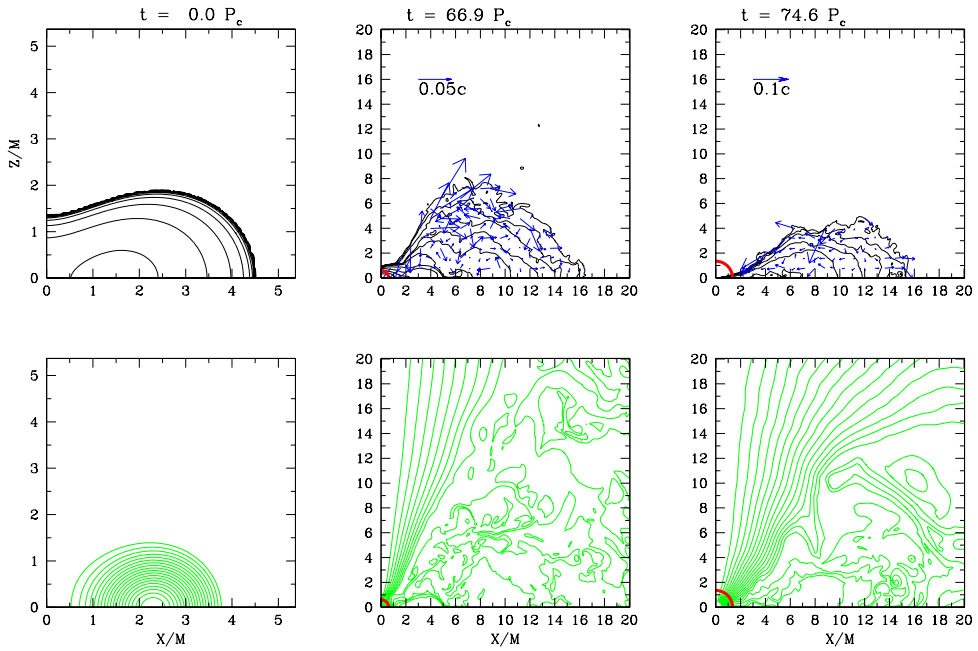

FIGURE 3. Collapse of a magnetized HMNS to a black hole. The upper 3 panels show snapshots of the rest-mass density contours and velocity vectors on the meridional plane. The lower panels show the field lines (lines of constant vector potential A_ϕ) for the poloidal magnetic field at the same times as the upper panels. The density contours are drawn for $\rho/\rho_{\rm max,0} = 10^{-0.3i-0.09}$ (i = 0–12). The field lines are drawn for $A_\phi = A_{\phi,\rm min} + (A_{\phi,\rm max} - A_{\phi,\rm min})i/20$ (i = 1–19), where $A_{\phi,\rm max}$ and $A_{\phi,\rm min}$ are the maximum and minimum value of A_ϕ respectively at the given time. The thick solid curves in the lower left corner denote the apparent horizon. [From Duez *et al.* 2006a.]

short-hard GRBs have characteristic timescales in the range $\tau \sim$ 10ms $-$2s. They are identified in low star-forming regions (ellipticals) where associations with supernovae can be excluded. The favored model for their progenitors are either NSNS or BHNS mergers. Alternative routes by which NSNS mergers can result in the generation of a short-hard GRB are traced in Fig. 4. These alternatives have emerged from detailed simulations in general relativity. The HMNS route has already been summarized in Section 3.

The inspiral and merger of NSNSs and BHNSs have important implications for the detection of gravitational waves with Advanced LIGO. Recent estimates for the rates for detectable NSNS mergers are promising, in the neighborhood of $20-30{\rm yr}^{-1}$ (O'Shaughnessy *et al.* 2006). Simulations in general relativity now underway should be helpful in preparing for the exciting possibility of the simultaneous detection of a gravitational wave *and* GRB from the *same* source in the near future.

5. Magnetorotational Collapse of Massive Stars to Black Holes

Recently, we performed simulations in axisymmetry of the magnetorotational collapse of very massive stars in full general relativity (Liu, Shapiro & Stephens 2007). Our simulations are directly applicable to the collapse of supermassive stars with masses $M \gtrsim 10^3 M_\odot$ and to very massive Population III stars. They are also relevant for core collapse in massive Population I stars, since in all of these cases the governing EOS up to the appearance of a black hole can be approximated by an adiabatic $\Gamma = 4/3$

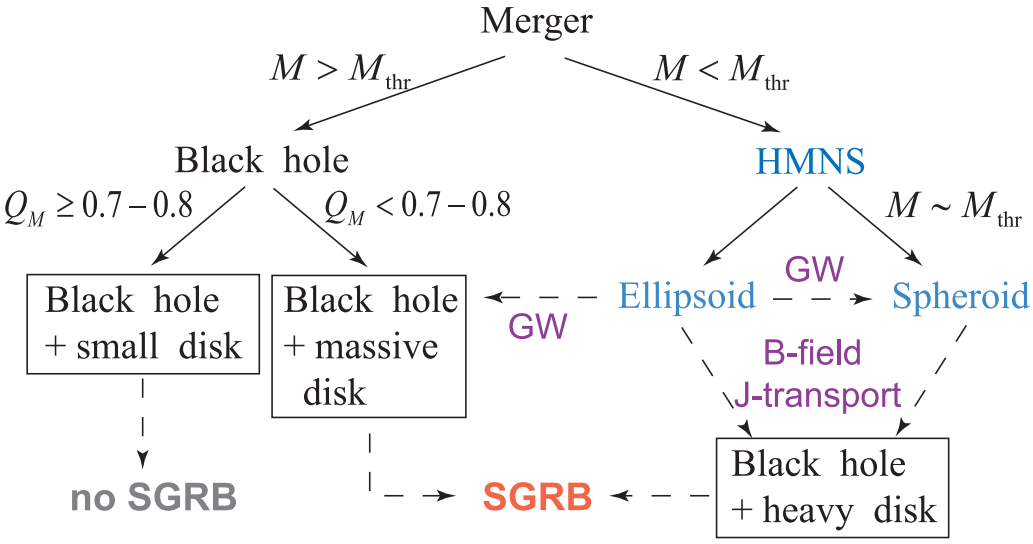

FIGURE 4. Plausible routes for the formation of a short-hard gamma-ray burst (SGRB) central engine following the merger of a binary neutron star. Here "GW" ("B-field J-transport") denotes angular momentum dissipation dominated by gravitational wave emission (magnetic fields). [From Shibata & Taniguchi 2006.]

law (although its physical origin is different). These simulations may help explain the formation of the central engine in the collapsar model of long-soft GRBs (MacFadyen & Woosley 1999). Moreover, some long-soft GRBs observed at very high redshift might be related to the gravitational collapse of very massive Pop III stars (Schneider, Guetta & Ferrara 2002, Bromm & Loeb 2006). Hence these simulations may also provide direct insights into the formation of GRB central engines arising from first-generation stars.

The simulations of Liu, Shapiro & Stephens (2007) model the initial configurations by $n = 3$ polytropes, uniformly rotating near the mass-shedding limit and at the onset of radial instability to collapse. These simulations extend the earlier results of Shibata & Shapiro 2002 by incorporating the effects of a magnetic field and by tracking the evolution for a much longer time after the appearance of a central black hole. The ratio of magnetic to rotational kinetic energy in the initial stars is chosen to be small (1% and 10%). We find that such magnetic fields do not affect the *initial* collapse significantly. The core collapses to a black hole, after which black hole excision is employed to continue the evolution long enough for the hole reach a quasi-stationary state. We find that the black hole mass is $M_h = 0.95M$ and its spin parameter is $J_h/M_h^2 = 0.7$, with the remaining matter forming a torus around the black hole. The *subsequent* evolution of the torus does depend on the strength of the magnetic field. We freeze the spacetime metric ("Cowling approximation") and continue to follow the evolution of the torus after the black hole has relaxed to quasi-stationary equilibrium. In the absence of magnetic fields, the torus settles down following ejection of a small amount of matter due to shock heating. When magnetic fields are present, the field lines gradually collimate along the hole's rotation axis. MHD shocks and the MRI generate MHD turbulence in the the torus and stochastic accretion onto the central black hole (see Fig. 5). When the magnetic field is strong, a wind is generated in the torus, and the torus undergoes radial oscillations that drive episodic accretion onto the hole. These oscillations produce long-wavelength gravitational waves potentially detectable by LISA. The final state of magnetorotational collapse always consists of a central black hole surrounded by a collimated magnetic field

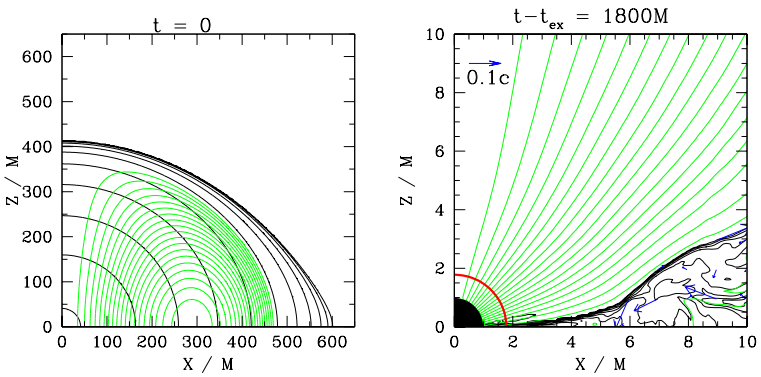

FIGURE 5. Magnetoroational collapse of a massive star to a black hole. Snapshots of meridional rest-mass density contours, velocity vectors and poloidal magnetic field lines for the initial and endpoint configurations for $n = 3$ collapse. Field lines coincide with contours of vector potential A_φ and are drawn for $A_\varphi = A_{\varphi,\max}(j/20)$ with $j = 1, 2, \cdots, 19$ where $A_{\varphi,\max}$ is the maximum value of A_φ. In the final, post-excision model ($t_{\rm ex} = 29150M$), the density levels are drawn for $\rho_0 = 100\rho_c(0)10^{-0.3j}$ (j = 0–10). The thick arc near the lower left corner of the right-hand frame denotes the apparent horizon and the shaded region the excision domain. [Adapted from Liu, Shapiro & Stephens 2007.]

and a hot, thick accretion torus. This system is a viable candidate for the central engine of a long-soft gamma-ray burst.

6. Cosmological Growth of Supermassive Black Holes

Growing evidence indicates that supermassive black holes (SMBHs) with masses in the range $10^6 - 10^{10}M_\odot$ exist and are the engines that power AGNs and quasars. There is also ample evidence that SMBHs reside at the centers of many, and perhaps most, galaxies, including the Milky Way. The highest redshift of a quasar discovered to date is $Z_{\rm QSO} = 6.43$, corresponding to QSO SDSS 1148+5251 (Fan *et al.* 2003). Accordingly, if they are the energy sources in quasars (QSOs), the first SMBHs must have formed prior to $Z_{\rm QSO} = 6.43$, or within $t = 0.87$ Gyr after the Big Bang in the concordance ΛCDM cosmological model. This requirement sets a significant constraint on black hole seed formation and growth mechanisms in the early universe. Once formed, black holes grow by a combination of mergers and gas accretion.

The more massive the initial seed, the less time is required for it to grow to SMBH scale and the easier it is to have a SMBH in place by $Z \geqslant 6.43$. One possible progenitor that readily produces a SMBH is a supermassive star (SMS) with $M \gg 10^3M_\odot$ (Rees 1984, Shapiro 2004). SMSs can form when gaseous structures build up sufficient radiation pressure to inhibit fragmentation and prevent normal star formation; plausible cosmological scenarios have been proposed that can lead to this situation (Gnedin 2001, Bromm & Loeb 2003). Alternatively, the seed black holes that later grow to become SMBHs may originate from the collapse of Pop III stars $\lesssim 10^3M_\odot$ (Madau & Rees 2001). To achieve the required growth to $\sim 10^9M_\odot$ by $Z_{\rm QSO} \gtrsim 6.43$, it may be necessary for gas accretion, if restricted by the Eddington limiting luminosity, to occur at relatively *low* efficiency of rest-mass to radiation energy conversion ($\lesssim 0.2$; Shapiro 2005 and references therein), as we discuss below.

The efficiency of black hole accretion, and the resulting rate of black hole growth, is significantly affected by the spin of the black hole. The spin evolution of a black hole

a/M	ϵ_M	Spin Equilibrium?	Characterization
0.0	0.057	no	standard thin disk; nonspinning BH
0.95	0.19	yes	turbulent MHD disk
0.998	0.32	yes	standard thin disk; photon recapture
1.0	0.42	yes	standard thin disk; max spin BH

TABLE 1. Rest-mass-to-radiation conversion efficiency *vs.* black hole spin.

begins at birth. If the hole arises from the collapse of a massive or supermassive star, then it is likely to be born with a spin parmeter in the range $0 \leqslant a/M \lesssim 0.8$. The lower limit applies if the progenitor star (or core) is nonrotating, the upper limit if it is spinning uniformly at the mass-shedding limit at the onset of collapse, as found in the simulations of Shibata & Shapiro and Liu & Shapiro 2007 and discussed in Section 5. Major mergers with other black holes of comparable mass will cause the black hole to spin up suddenly to $a/m \approx 0.8 - 0.9$, as the merged remnant acquires almost all of the mass and angular momentum that characterizes a circular orbit, quasistationary BHBH binary at the innermost stable circular orbit (ISCO). Once secular gravitational radiation loss drives the binary past the ISCO, the black holes undergo a rapid dynamical plunge and coalescence, with little additional loss of energy and angular momentum.. This anticipated behavior has now been confirmed by numerical simulations of BHBH mergers (see Centrella 2007, This Volume, and references therein). These simulations also show that gravitational radiation reaction can induce a large kick velocity ($\gtrsim 1000$ km/s) in the remnants following mergers. While in principle these large kick velocities pose a great hazard for the growth of black hole seeds to SMBHs by $Z \sim 6$, large kicks are possible only if the spins of the black hole binary companions are appreciable and their masses are comparable. In the end, gravitational recoil does not pose a significant threat to the formation of the SMBH population observed locally, although high mass seeds are favored (Volonteri 2007).

Minor mergers with many smaller black holes, isotropically distributed, cause the black hole to spin down: $a/m \sim M^{-7/3}$ (Hughes & Blandford 2003, Gammie, Shapiro & McKinney 2004). The reason is that the ISCO and specific angular momentum of black holes orbiting counter-clockwise is larger than for holes orbiting clockwise, hence the net effect of isotropic capture is spindown.

However, it is likely that most of the mass of a supermassive black hole has been acquired by gas accretion, not mergers. Such a conclusion can be inferred from the observation that the luminosity density of quasars is roughly $0.1 - 0.2$ of the local SMBH mass density (Soltan 1982, Yu & Tremaine 2002), an equality that arises naturally from growth via gaseous disk accretion. Steady gas accretion will quickly drive the black hole to spin equilibrium, with a spin parameter that depends on the nature of the flow. If accretion occurs via a relativistic "standard thin disk", then the hole will be driven to the Kerr limiting value, $a/M = 1$ (Bardeen 1970). Correcting for the recapture of some of the emitted photons from such a disk reduces the equilibrium spin value to 0.998 (Thorne 1974). If, however, the accretion is driven by MRI turbulence in a relativistic MHD disk, then recent simulations indicate (McKinney & Gammie 2004, Gammie, Shapiro & McKinney 2004, De Villiers *et al.* 2005) that the equilibrium spin will fall to ~ 0.95. The small differences between these equilibrium spin parameters is deceptive, for they correspond to very different rest-mass-to-radiation conversion efficiencies, as shown in Table 1.

The significance of these different values is that the growth of a black hole with time via steady accretion depends *exponentially*, on the rest-mass-to-radiation conversion efficiency, ϵ_M, as we will now recall. Define the rest-mass-to-radiation conversion efficiency ϵ_M and the luminosity efficiency ϵ_L according to

$$\epsilon_M \equiv L/\dot{M}_0 c^2 = \epsilon_M(a/M) \quad \epsilon_L \equiv L/L_E \tag{6.1}$$

where M is the black hole mass, M_0 is the accreted rest-mass, and L_E is the Eddington luminosity given by

$$L_E = \frac{4\pi M \mu_e m_p c}{\sigma_T} \approx 1.3 \times 10^{46} \mu_e M_8 \text{ erg s}^{-1} \ . \tag{6.2}$$

Here τ is the growth timescale,

$$\tau = \frac{Mc^2}{L_E} \approx 0.45 \mu_e^{-1} \text{ Gyr} \ , \tag{6.3}$$

and μ_e is the mean molecular weight per electron. With the above definitions the growth rate of a black hole due to accretion is

$$\frac{dM}{dt} = (1-\epsilon_M)\frac{dM_0}{dt} = \left[\frac{\epsilon_L(1-\epsilon_M)}{\epsilon_M}\right]\frac{M}{\tau} \ . \tag{6.4}$$

Integrating equation (6.4) for steady accretion with constant efficiencies trivially yields the mass amplification of a black hole with time,

$$M(t)/M(t_i) = \exp\left[\frac{\epsilon_L(1-\epsilon_M)}{\epsilon_M}\frac{(t-t_i)}{\tau}\right] \ , \tag{6.5}$$

showing the exponential dependence on the efficiency factors.

Now a possible clue to the upper limit of ϵ_L is provided by the broad-line quasars in a Sloan Digital Sky Survey sample of 12,698 nearby quasars in the redshift interval $0.1 \leqslant z \leqslant 2.1$. This survey supports the value $\epsilon_L \approx 1$ as a physical upper limit (McLure & Dunlop 2004). Hence to maximize mass amplification via steady accretion, one must accrete with a small value of ϵ_M at the Eddington limit, $\epsilon_L \approx 1$.

Fig. 6 evaluates equation (6.5) for black hole seeds that form at redshift Z_i from the collapse of Pop III stars in the range $100 \lesssim M/M_\odot \lesssim 600$, and subsequently grow to $10^9 M_\odot$ by $Z_{\rm QSO} = 6.43$. The ΛCDM concordance cosmological model is assumed. Of particular relevance is the case of "merger-assisted" mass amplification, whereby mergers account for a typical growth of $\sim 10^4$ in black hole mass, the remainder being by gas accretion (see, e.g., Yoo & Miralda-Éscude 2004). The figure shows that for $Z_i \gtrsim 40$, the required growth of the seed to SMBH status is easily achieved for a relativistic MHD accretion disk, but is only marginally possible for a standard thin disk that accounts for photon recapture, and not at all possible for a standard thin disk that drives the black hole to maximal spin. However, if the initial black hole seed is less than $600 M_\odot$, accretion via a standard thin disk appears to be ruled out altogether. The fact that a black hole driven to spin equilibrium by a turbulent MHD disk accretes with low enough efficiency to grow to supermassive size by $Z_{\rm QSO} \approx 6.43$ is potentially significant. It points to the need for further relativistic MHD simulations of black hole accretion with ever greater physical sophistication, including the full effects of radiation transfer.

These same conclusions also hold if the black hole seed forms much earlier than $Z_i \approx 40$, and they may be tightened if the seed forms later. In fact, it may be likely that the seed forms later, at $Z_i \lesssim 40$, given that even $4-\sigma$ peaks in the density perturbation spectrum for the progenitor halo of SDSS 1148+5251 do not collapse until $Z \sim 30$ in the

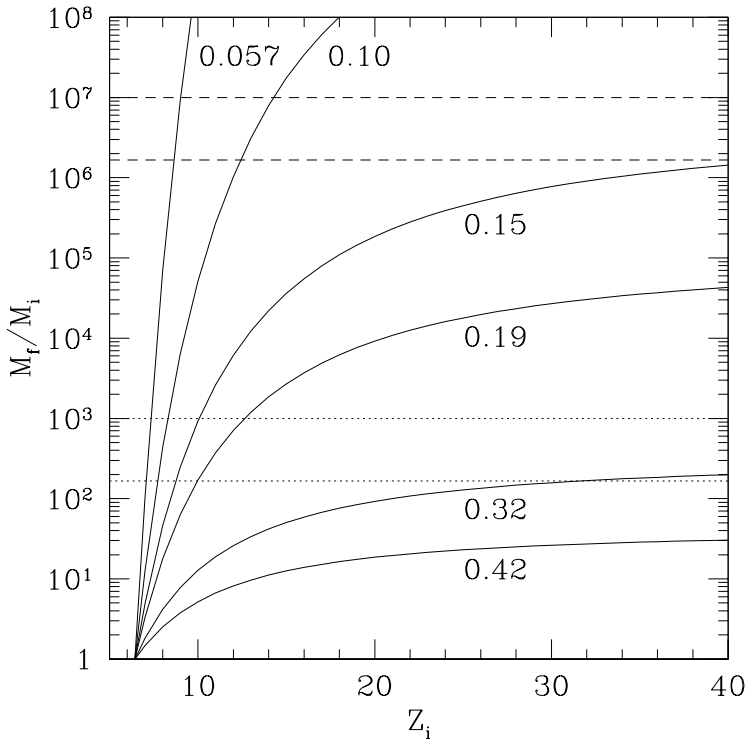

FIGURE 6. Black hole accretion mass amplification M_f/M_i versus redshift Z_i of the initial seed. Here we plot the amplification achieved by redshift $Z_f = 6.43$, the highest known quasar redshift, corresponding to 1148+5251. Each solid curve is labeled by the adopted constant radiation efficiency, ϵ_M; the luminosity is assumed to be the Eddington value ($\epsilon_L = 1$). The horizontal dashed lines bracket the range of amplification required for accretion alone to grow a seed black hole of mass $100 \leqslant M/M_\odot \leqslant 600$ formed from the collapse of a Pop III star to $10^9 M_\odot$. The horizontal dotted lines bracket the required accretion amplification range assuming that mergers account for a growth of 10^4 in black hole mass, the remainder being by gas accretion. [From Shapiro 2005.]

ΛCDM concordance cosmology (see, e.g. Figure 5 in Barkana & Loeb 2001.) Moreover, the potential wells of the earliest halos are quite shallow (~ 1 km/s) and may not be able to retain enough gas to form stars. Nevertheless, the effect of altering the date of birth of the black hole seed is not very great unless $Z_i \lesssim 20 - 25$, as is evident from Fig. 3.

Should a quasar be discoverd at $Z_{\rm QSO}$ substantially above 6.43, it would not be understood easily in the context of supermassive black hole growth by gas accretion from a seed arising from the collapse of a stellar-mass, Pop III progenitor.

The analysis presented here is illustrative only; the results may change as the treatment is refined. The main point of this example is to emphasize that our understanding of structure formation in the early universe as it pertains to the formation and growth of supermassive black holes (global physics) depends in part on resolving some of the important details of relativistic BHBH recoil and relativistic black hole accretion (local physics). To understand these details, in turn, requires large-scale simulations in full general relativity, which are now possible and underway.

7. Conclusions

We have discussed a number of black hole scenarios that require numerical simulations in full general relativity for true understanding. Some of these processes involve the formation of black holes, others concern their subsequent growth and interactions. The important point is that numerical relativity is at last mature enough to probe these issues reliably. Numerical relativity can now serve as an important tool to simulate stellar collapse to black holes, the inspiral, merger and recoil of BHBHs, NSNSs and BHNSs, the generation of gravitational waves from stellar collapse and binary mergers, accretion onto black holes, and countless other phenomena involving black holes and their strong gravitational fields. With such a tool, these processes now can be investigated at a fundamental level without many of the ad hoc assumptions and approximations required in previous treatments. This should lead to an improved qualitative picture, as well as more reliable quantitative results.

We are grateful to T. Baumgarte, C. Gammie, Y-T Liu, and M. Shibata for useful discussions. S.L.S is supported by NSF grants PHY-0205155, PHY-0345151, and PHY-0650377 and NASA Grants NNG04GK54G and NNX07AG96G to the University of Illinois.

REFERENCES

Arnowitt, R, Deser, S. & Misner, C. W. 1962 Canonical analysis of general relativity. In *Gravitation: An Introduction to Current Research* (ed. L. Witten). Wiley, New York, p. 127.

Baker, J. G., Centrella, J., Choi, D. I., Koppitz, M. & van Meter, J. 2006 Gravitational-wave extraction from an inspiraling configuration of merging black holes. *Phys. Rev. Lett.* **96**, 11102.

Balbus, S. A. & Hawley, J. P. 1991 A powerful local shear instability in weakly magnetized disks. I - Linear analysis. II - Nonlinear evolution. *Astrophs. J.* **376**, 214-233.

Balbus, S. A. & Hawley, J. P. 1998 Instability, turbulence, and enhanced transport in accretion disks. *Rev. Mod. Phys.* **70**, 1-53.

Bardeen, J. M. 1970 Kerr metric black holes. *Nature* **226**, 64.

Barkana, R. & Loeb, A. 2001 In the beginning: the first sources of light and the reionization of the universe. *Phys. Repts.* **349**, 125-238.

Baumgarte, T. W. & Shapiro, S. L. 1999 Numerical integration of Einstein's field equations. *Phys. Rev. D.* **59**, 024007.

Baumgarte, T. W. & Shapiro, S. L. 2003 Numerical relativity and compact binaries. *Phys. Repts.* **376**, 41-131.

Baumgarte, T. W., Shapiro, S. L. & Shibata, M. 2000 On the maximum mass of differentially rotating neutron stars. *Astrophys. J. Lett.* **528**, L29-L32.

Bromm, V. & Loeb, A. 2003 Formation of the first supermassive black holes. *Astrophys. J.* **596**, 34-46.

Bromm, V. & Loeb, A. 2006 High-redshift gamma-ray bursts from Population III progenitors. *Astrophys. J.* **642**, 382-388.

Campanelli, M., Lousto, C. O., Marronetti, P. & Zlochower, Y. 2006 Accurate evolutions of orbiting black-hole binaries without excision. *Phys. Rev. Lett* **96**, 111101.

Chandrasekhar, S. 1960 The Stability of Non-Dissipative Couette Flow in Hydromagnetics. *Proc. Nat. Acad. Sci.* **46**, 253-257.

Cook, J. N., Shapiro, S. L. & Stephens, B. C. 2003 Magnetic Braking and Viscous Damping of Differential Rotation in Cylindrical Stars *Astrophys. J.* **599**, 1272-1292.

De Villiers, J.-P., Hawley, J. F., Krolik, J. H. & Hirose, S. 2005 Magnetically driven accretion in the Kerr metric. III. Unbound outflows. Astrophys. J. **620**, 878-888.

Duez, M. D., Liu, Y. T., Shapiro, S. L. & Stephens, B. C. 2005 Relativistic magnetohydrodynamics in dynamical spacetimes: Numerical methods and tests. *Phys. Rev. D.* **72**, 024028.

Duez, M. D., Liu, Y. T., Shapiro, S. L., Shibata, M. & Stephens, B. C. 2006a Collapse of magnetized hypermassive neutron stars in general relativity. *Phys. Rev. Lett.* **96**, 031101.

Duez, M. D., Liu, Y. T., Shapiro, S. L., Shibata, M. & Stephens, B. C. 2006b Evolution of magnetized, differentially rotating neutron stars: Simulations in full general relativity. *Phys. Rev. D.* **73**, 104015.

Duez, M. D., Shapiro, S. L. & Yo, H.-J. 2004 Relativistic hydrodynamic evolutions with black hole excision. *Phys. Rev. D.* **69**, 104016.

Faber, J. A., Grandclément, P. & Rasio, F. A. 2004 Mergers of irrotational neutron star binaries in conformally flat gravity. *Phys. Rev. D.* **69**, 124038.

Faber, J. A. & Rasio, F. A. 2000 Post-Newtonian SPH calculations of binary neutron star coalescence: Method and first results *Phys. Rev. D.* **62**, 064012.

Faber, J. A. & Rasio, F. A. 2002 Post-Newtonian SPH calculations of binary neutron star coalescence. III. Irrotational systems and gravitational wave spectra. *Phys. Rev. D.* **65**, 084042.

Fan, X. *et al.* 2003 A Survey of $z > 5.7$ quasars in the Sloan Digital Sky Survey. II. Discovery of three additional quasars at $z > 6$. *Astron. J.* **125**, 1649-1659.

Gammie, C. F., Shapiro, S. L. & McKinney 2004 Black hole spin evolution. *Astrophys. J.* **602**, 312-319.

Gnedin, O. Y. 2001 Million solar mass black holes at high redshift. *Class. Quan. Grav.* **18**, 3983-3988.

Hughes, S. A. & Blandford, R. D. 2003 Black hole mass and spin coevolution by mergers. *Astrophys. J. Lett.* **585**, L101-104.

Lichnerowicz, A. 1944 The integration of the relativistic gravitation equations and the problem of N bodies. *J. Math. Pure Appl.* **23**, 37-63.

Liu, Y. T. & Shapiro, S. L. 2004 Magnetic braking in differentially rotating, relativistic stars *Phys. Rev. D.* **69**, 044009/1-27.

Liu, Y. T., Shapiro, S. L. & Stephens, B. 2007 Magnetorotational collapse of very massive stars in full general relativity. *astro-ph/0706.2360*

MacFadyen, A. I. & Woosley, S. E. 1999 Collapsars: Gamma-ray bursts and explosions in "failed supernovae *Astrophys. J.* **524**, 262-289.

Madau, P. & Rees, M. 2001 Massive black holes as Population III remnants. *Astrophys. J. Lett.* **551**, L27-L30.

McKinney, J. C. & Gammie, C. F. 2004 A measurement of the electromagnetic luminosity of a Kerr black hole. *Astrophys. J.* **611**, 977-995.

Mclure, R. J. & Dunlop, J. S. 2004 The cosmological evolution of quasar black hole masses. *MNRAS* **352**, 1390-1404.

Morrison, I. A., Baumgarte, T. W. & Shapiro, S. L. 2004 Effect of differential rotation on the maximum mass of neutron stars: realistic nuclear equations of state. *Astrophys. J.* **610**, 941-947.

Nice, D. J., Splaver, E. M., Stairs, I. H., Löhmer, O., Jessner, A., Kramer, M. & Cordes, J. M. 2005 A $2.1 M_\odot$ Pulsar Measured by Relativistic Orbital Decay *Astrophys. J.* **634**, 1242-1249.

O'Shaughnessy, R., Kim, C., Kalogera, V. & Belczynski, K. 2006 Constraining population synthesis models via observations of compact-object binaries and supernovae *astro-ph/0610076*

Pretorius, F. 2005 Evolution of binary black-hole spacetimes. *Phys. Rev. Lett.* **95**, 121101.

Rasio, F. A. & Shapiro, S. L. 1994 Hydrodynamics of binary coalescence. 1: Polytropes with stiff equations of state. *Astrophys. J.* **432**, 242-261.

Rasio, F. A. & Shapiro, S. L. 1999 Coalescing binary neutron stars. *Class. Quant. Grav.* **16**, R1-R29.

Rees, M. J. 1984 Black hole models for active galactic nuclei. *Ann. Rev. Astro. ApJ.* **22**, 471-506.

Saijo, M., Shibata, M., Baumgarte, T. W. & Shapiro, S. L. 2001 Dynamical bar instability in rotating Stars: effect of general relativity. *Astrophys. J.* **548**, 991-931.

Schneider, R., Guetta, D. & Ferrara, A. 2002 Gamma-ray bursts from the first stars: neutrino signals. *MNRAS* **334**, 173-181.

Shapiro, S. L. 2000 Differential rotation in neutron stars: Magnetic braking and viscous damping. *Astrophys. J.* **544**, 397-408.

Shapiro, S. L. 2004 Formation of supermassive black holes: Simulations in general relativity. In *Carnegie Observatories Astrophysics Series, Vol I: Coevolution of Black Holes and Galaxies* (ed. L. C. Ho). Cambridge Univ. Press, Cambridge, p. 103.

Shapiro 2005 2005 Spin, accretion and the cosmological growth of supermassive black holes. *Astrophys. J.* **620**, 59-68.

Shibata, M. 2005 Constraining Nuclear Equations of State Using Gravitational Waves from Hypermassive Neutron Stars. *Phys. Rev. Lett.* **94**, 201101.

Shibata, M., Baumgarte, T. W. & Shapiro, S.L. 2000 The bar-mode instability in differentially rotating neutron stars: simulations in full general relativity. *Astrophys. J.* **542**, 453-463.

Shibata, M., Duez, M. D., Liu, Y. T., Shapiro, S. L. & Stephens, B. C. Magnetized hypermassive neutron-star collapse: A central engine for short gamma-ray bursts" *Phys. Rev. Lett* **96**, 031102.

Shibata, M. & Nakamura, T. 1995 Evolution of three-dimensional gravitational waves: Harmonic slicing case. *Phys. Rev. D.* **52**, 5428.

Shibata, M. & Sekiguchi, Y. I. 2005 Magnetohydrodynamics in full general relativity: Formulation and tests. *Phys. Rev. D.* **72**, 044014.

Shibata, M. & Shapiro, S. L. 2002 Collapse of a rotating supermassive star to a supermassive black hole: Fully relativistic simulations. *Astrophys. J. Lett.* **572**, L39-L43.

Shibata, M. & Taniguchi, K. 2006 Merger of binary neutron stars to a black hole: Disk mass, short gamma-ray bursts, and quasinormal mode ringing. *Phys. Rev. D.* **73**, 064027.

Shibata, M., Taniguchi, K. & Uryū, K. 2003 Merger of binary neutron stars of unequal mass in full general relativity. *Phys. Rev. D.* **68**, 084020.

Shibata, M., Taniguchi, K. & Uryū, K. 2005 Merger of binary neutron stars with realistic equations of state in full general relativity. *Phys. Rev. D.* **71**, 084021.

Soltan, A.1982 Masses of quasars. *MNRAS* **200**, 115-122.

Stairs, I. H. 2004 Pulsars in binary systems: probing binary stellar evolution and general relativity. *Science* **304**, 547-552.

Thorne, K. S. 1974 Disk-accretion onto a black hole. II. Evolution of the hole. *Astrophys. J.* **191**, 507-520.

Thorsett, S. E. & Chakrabarty, D. 1999 Neutron star mass measurements. I. Radio pulsars. *Astrophys. J.* **512**, 288-299.

Velikhov, E. P. 1959 Stability of an ideally conducting liquid flowing between cylinders rotating in a magnetic field *Sov. Phys.-JETP* **232**, 995.

Volonteri, M. 2007 Gravitational recoil: Signatures on the massive black hole population. *Astrophys. J. Lett.* **663**, L5-L8.

Yoo, J. & Miralda-Escude, J. 2004 Formation of the black holes in the highest redshift quasars. *Astrophys. J. Lett* **614**, L25-L28.

York, J. W., Jr. 1971 Gravitational degrees of freedom and the initial-value problem. *Phys. Rev. Lett.* **26**, 1656-1658.

Yu, Q. & Tremaine, S. 2002 Observational constraints on growth of massive black holes. *MNRAS* **335**, 965-976.

Zhuge, X., Centrella, J. M. & McMillan, S. L. W. 1996 Gravitational radiation from the coalescence of binary neutron stars: Effects due to the equation of state, spin, and mass ratio. *Phys. Rev. D.* **54**, 7261-7277.